Robert Cox; Lt. James P. Mosman, USN; LCdr. Duncan McKay, USN;
Dr. Steven B. Leeb; Cdr. Timothy J. McCoy, USN

Diagnostic Indicators for Shipboard Cycling Systems Using Non-Intrusive Load Monitoring

ABSTRACT

Field studies have demonstrated that it is possible to evaluate the state of many shipboard systems by analyzing the electrical power that is drawn by electromechanical actuators (Ramsey, 2005; DeNucci, 2005; Greene, 2005). This paper describes how a device known as a non-intrusive load monitor (NILM) uses electrical power measurements to detect the presence of leaks in shipboard cycling systems. A cycling system model is presented, and this model is used to develop several diagnostic indicators. These indicators are demonstrated using both simulated data and field data obtained aboard the *USCGC Seneca* (*WMEC-906*).

INTRODUCTION

Given the sharp rise in the number and complexity of shipboard systems, the U.S. Navy has developed a clear need for reliable, automated condition-based maintenance (CBM) systems. Although this demand has been partially met through the development of the Integrated Condition Assessment System (ICAS), there is still significant room for improvement (DiUlio, 2003). For example, ICAS currently relies on data obtained manually from thousands of remote sensors (DiUlio, 2003). This monitoring scenario has several very serious shortcomings. First, the use of a large sensor network creates an entirely new set of maintenance issues, as each sensor added to the network also becomes a new point of failure. Additionally, the use of manual data collection is in direct conflict with the Navy's current desire to reduce shipboard manning. Furthermore, any effort to introduce automated data collection on a large scale will require thousands of feet of new cabling or many small wireless modules, which will only further exacerbate current reliability issues and drive up installation costs. As shown in (DeNucci, et al 2005), the shipboard CBM process can be greatly simplified through the use of a non-intrusive load monitor (NILM), which is a device that can assess the performance of each of the major loads on an electrical service using only measurements of the input voltage and aggregate load current. In this paper, we demonstrate how the NILM can use its small set of electrical measurements to assess the performance of shipboard cycling systems.

In the sections that follow, we describe the process by which we developed a successful diagnostic indicator for shipboard cycling systems. We begin by describing the fundamental features of such systems, and we then describe how a NILM can be used to study them. Next, we develop a model that adequately describes the behavior of the system, and we demonstrate how fault conditions affect the behavior of that model. Using the results obtained from our model simulations, we then propose several diagnostic indicators that can be used to detect system faults. Finally, we demonstrate the efficacy of our diagnostic indicators using field measurements performed using the vacuum-assisted waste disposal system aboard the *USCGC Seneca*.

CYCLING SYSTEMS

Naval vessels commonly use compressed air or vacuum systems to perform a number of critical functions, including waste collection and pneumatic valve actuation. To ensure instant availability and to provide for short periods of high demand, these systems typically have a pressure tank that is periodically charged by an electrically actuated compressor or pump. A typical layout is shown in Figure 1. As loads draw from the reservoir, system pressure decreases. Once a certain low pressure set point has been reached, the controller will transmit a

start command to the pump or compressor, causing the device to begin charging the system. Once the pressure has reached the predetermined high set point, the pump motors are either de-energized or the pumps are directed to enter a re-circulation mode. From an electrical perspective, this behavior creates a *cycling system* in which electrical power usage follows a regular cycle of charging and discharging based on a pressure.

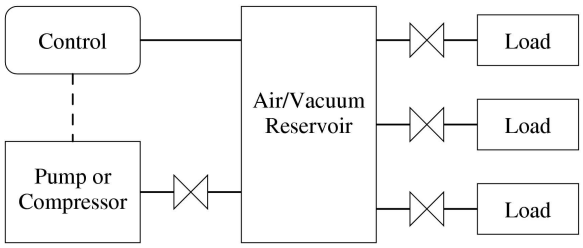

Figure 1: Diagram of a typical cycling system. Solid lines indicate air paths, and dotted lines indicate electrical connections.

Given the clear relationship that exists between pump power consumption and reservoir pressure, cycling systems are perfectly suited for non-intrusive monitoring. A typical measurement configuration is shown in Fig. 2. In that arrangement, the NILM measures the current flowing to a bank of electrical loads, one or more of which are the pumps or compressors in the target cycling system. Using measurements of the voltage and current, a software-based *preprocessor* onboard the NILM computes the real and reactive power drawn by each of the loads on the electrical service. Once the real power has been computed, it is passed to an event detector that identifies the operation of each of individual loads on the monitored electrical service by matching a series of templates, or exemplars, to each of the observed transients. Figure 3 shows the successful identification of a pump servicing the vacuum-assisted waste disposal system aboard the *USCGC Seneca*. Complete details of the NILM's preprocessor and transient event detector can be found in (Shaw, 2000).

The final task performed by a NILM device is to pass the pump power data to a diagnostics module that assesses the current operational status of the target cycling system. In order to make that assessment, the diagnostics module must be provided with a model that explains how individual loads in the cycling system affect the measured pump power. The importance of such a model is demonstrated in Fig. 4, which shows both pressure and pump power in a representative cycling system located aboard the *Seneca*. As shown, any time that a system usage event (SUE) removes vacuum from the system, a sharp drop is observed in the measured pressure. Note that if either the size or the number of SUEs increases, the discharge period will shorten and the number of pump runs will increase. Further, as the data in Fig. 4 suggests, the presence of a leak or a persistent load causes a steady, background vacuum loss. As a result, there is again an increase in the number of pump runs and a decrease in the average length of a discharge period. Without a system model, it is impossible to use measurements of the pump power to distinguish between these two very different sets of events. In the next section, we develop a model that makes this distinction possible.

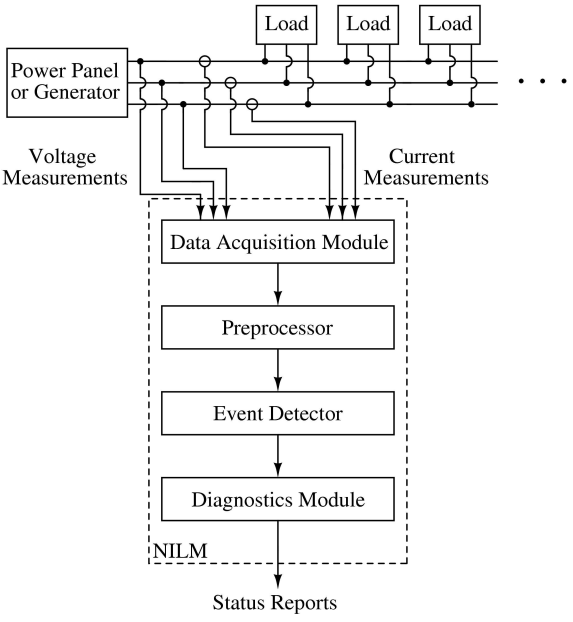

Figure 2: Diagram showing the fundamental signal flow path in a NILM. The final status report is sent electronically to the ship's Engineering Officer.

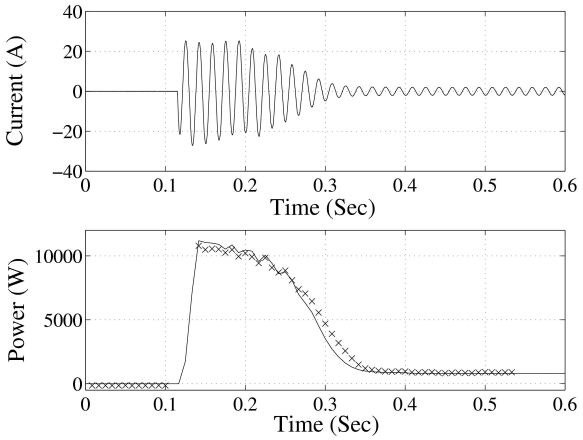

Figure 3: Measured current and computed power during the start of 1.7hp vacuum pump motor. Also shown in the power plot is a section of the template that has been successfully matched to the observed transient behavior.

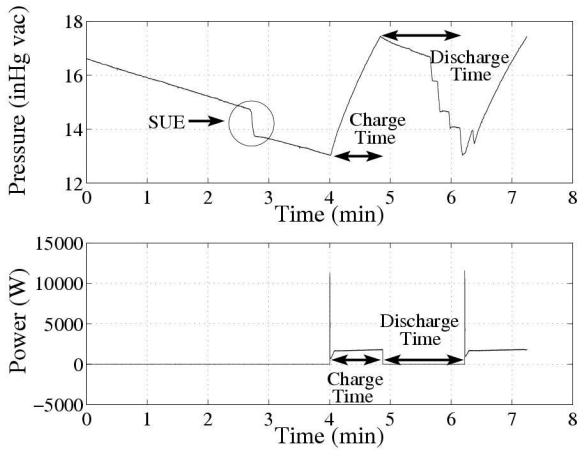

Figure 4: Reservoir pressure and pump input power during several charge and discharge cycles in the vacuum-assisted waste disposal system aboard *Seneca*. Note that the sharp drops in pressure are the direct results of system usage events (SUEs) and that the persistent background loss is the result of a small leak.

CYCLING SYSTEM MODEL

The cycling system model presented in this paper describes how the characteristics of the system's various air loads determine the operating schedule of its pumping device. To explain this critical relationship, the model describes how individual air loads affect the pressure in the reservoir, which is the physical quantity that the pumping devices are attempting to control. The complete model thus accounts for both the dynamics of the loads of interest as well as the rate at which individual loads impact the system. In general, the specifics of these two key components of the basic model will differ from one system to the next; regardless, once one constructs a specific cycling system model, it is easy to adapt it to reflect the characteristics of other, similar systems. In this section, we describe the major components of the general cycling system model in the context of a vacuum-assisted waste disposal system. This particular example highlights the information that must be considered when adapting the general model to a specific case.

Pneumatic Load Dynamics

In a typical cycling system, the pumps will charge the reservoir to a predetermined high pressure set point, denoted as P_{high}. In general, the reservoir pressure, $P(t)$, will decrease in response to both persistent loads and short-time air demands (e.g. SUEs). Thus, at any given moment during a single discharge period, $P(t)$ can be expressed in terms of several different quantities and effects, including the high pressure set point, the loss rate for all currently active loads, and the total loss caused by all loads that were active earlier in the same discharge period.

In vacuum-assisted waste disposal systems, there are two relevant types of pressure-removing events. The first of these are what we term system usage events, and they result from the operation of typical system air loads, such as drains. In general, these loads cause sharp, nearly instantaneous drops in reservoir pressure. In addition, we also consider leaks, which typically result in a persistent pressure loss. Assuming that the system can be accurately modeled using lumped element approximations, then the pressure loss due to a leak, which we denote as $P_{leak}(t)$, is the solution to the first order differential equation

$$\frac{dP}{dt} = -cP\,, \qquad (1)$$

where c is a constant whose value depends upon the parameters of the system. In later sections of

this paper, we will consider the solution to Eq. 1 as well as several reasonable approximations.

When these two types of events are both affecting the system, $P(t)$ can be approximated as

$$P(t) = P_{high} - (\Delta P_1 + \Delta P_2 + \Delta P_3 + \cdots + \Delta P_N) - P_{leak}(t) \quad (2)$$

where ΔP_k, is the pressure removed by the k-th SUE, $P_{leak}(t)$ is a functional description of the leak, and t=0 is defined to be the time at which the discharge period began. In order for the pumps to energize, the total pressure loss must be sufficient to cause $P(t)$ to fall below the controller's low pressure set point, P_{low}. Equivalently, the pumps will operate once the total pressure loss, ΔP_{loss}, is greater than the difference between P_{high} and P_{low}, i.e.

$$\Delta P_{loss} = \Delta P_1 + \Delta P_2 + \Delta P_3 + \cdots + \Delta P_N + P_{leak}(t) \geq P_{high} - P_{low}. \quad (3)$$

System Usage Process

The rate at which individual usage events affect the system has a strong impact on the operating schedule of the pumps. In general, however, these events occur at random intervals, as human or automated users typically operate the air loads only when needed. Thus, in order to describe system usage, one must propose an appropriate stochastic model. As shown below, one can determine a reasonably accurate model without performing a great deal of analysis and experimentation.

During our field studies aboard several active vessels, we have made extensive use of an arrival model known as an M/D/∞/∞ queue, which is appropriate in systems that have many independent users and many points in which those users can access the system (Tijms, 2003). As shown in (Tijms, 2003), the M/D/∞/∞ queue is equivalent to a Poisson process, which is often used to model natural arrival-type processes (Bertsekas, 2002). According to the Poisson model, the number of events $N(t)$ that occur in a time interval t is a Poisson-distributed random variable. When events arrive according to this probability law, it can be shown (Bertsekas, 2002) that the time T that elapses between successive arrivals is a random variable that is distributed according to the following probability density function (PDF):

$$f_T(t) = \lambda e^{-\lambda t}. \quad (4)$$

In general, the parameter λ, which is known as the arrival rate of the process, is itself a function of time. In this paper, we will consider both a constant λ, and a simple, time-dependent model that is based on both experimental findings and fundamental physical reasoning.

Pump Operating Schedule

The system usage and load models presented above can be used to predict how the pump's operating schedule will be affected by various operating conditions. In this section, we examine two different scenarios that have proven useful in developing a successful set of diagnostic indicators. In the first of these scenarios, we consider an idealized set of operating conditions, and in the second case, we modify those conditions so that the system's behavior reflects that of the *Seneca*'s waste disposal system. In each case, we demonstrate how leak conditions disturb the normal operating schedule of the system's pumping device. These test cases are used to motivate the diagnostic indicators that are presented later in this paper.

CASE 1: CONSTANT λ, CONSTANT ΔP

First, we consider a simple scenario in which each of the following conditions are satisfied:

- Each SUE reduces the reservoir pressure by an amount ΔP
- System usage is a homogeneous Poisson process, i.e. $\lambda(t) = \lambda$ (Bertsekas, 2002)
- The system usage process resets at the beginning of each discharge period

In this situation, the control relation presented in Eq. 2 can simplified to

$$P(t) = P_{high} - (\Delta P_1 + \Delta P_2 + \Delta P_3 + \cdots + \Delta P_N) - P_{leak}(t) = P_{high} - N\Delta P - P_{leak}(t). \quad (5)$$

If no leaks are present in the system, then this result can be simplified even further. With $P_{leak}(t) = 0$, we have

$$P(t) = P_{high} - N\Delta P \,. \quad (6)$$

Since ordinary usage is the only source of loss in Eq. 6, we know that the pump will energize as soon as $N\Delta P$ is large enough that $P(t) \le P_{low}$. Given that each SUE reduces $P(t)$ by the same amount, Eq. 6 clearly implies that there is a fixed number of usage events that must transpire before the controller will command the pump to energize. For instance, in the example system used to generate Fig. 5, it is clear that the pump will begin to operate immediately following the occurrence of the third SUE. For convenience, we define the variable N_{max}, which represents the maximum number of usage events that can occur during any single discharge period. As Fig. 5 implies, the value of N_{max} is simply the smallest integer that guarantees the validity of the inequality

$$P_{low} \ge P_{high} - N\Delta P \,. \quad (7)$$

Solving, we find that

$$N_{\max} = \left\lceil \frac{P_{high} - P_{low}}{\Delta P} \right\rceil, \quad (8)$$

where $\lceil x \rceil$ is the ceiling of x.

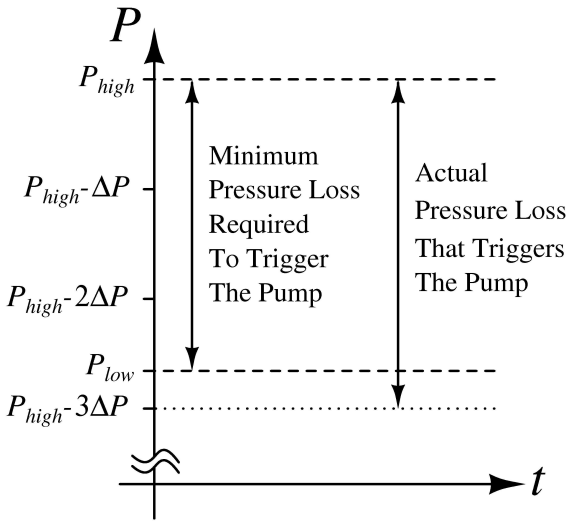

Figure 5: Key pressure values in an example cycling system in which N_{max}=3. As shown, the pump will energize as soon as the reservoir pressure drops below P_{low}, which, in this system, can only happen after the arrival of the third SUE.

When operating under the simplified conditions considered in this section, it is possible to predict the distribution for the time T_p that elapses during any individual discharge period. Given the fact that the number of usage events impacting the system is a fixed quantity, T_p is simply the sum of the N_{max} inter-arrival times, i.e.

$$T_p = T_1 + T_2 + \cdots + T_{N_{\max}} \,. \quad (9)$$

Because T_p is the sum of a fixed number of random variables, its PDF is given by the relation

$$f_{T_p}(t) = f_1(t) * f_2(t) * \cdots * f_{N_{\max}}(t) \,, \quad (10)$$

where * is the convolution operator (Bertsekas, 2002). Given the inter-arrival model presented in Eq. 4, the PDF for T_p is

$$f_{T_p}(t) = \frac{\lambda^{N_{\max}} t^{N_{\max}-1} e^{-\lambda t}}{(N_{\max}-1)!} \,. \quad (11)$$

A simulation was designed to validate the idealized behavior described in this section (DeNucci, 2005). The system parameters used in the simulation are presented in Table 1. Figure 6 shows the simulated frequency distribution for T_p, as well as the frequency distribution that is predicted by Eq. 11.

Table 1: Parameters used in the ideal system simulation.

Parameter	Value
P_{high}	17.5 inHg
P_{low}	13.5 inHg
λ	30 hr $^{-1}$
ΔP	1.1 inHg

In the event that the system develops a leak, its behavior will depart from that predicted above. A simple graphical explanation for this departure is presented in Fig. 7. As shown, the leak causes the reservoir pressure to decrease continuously. As a result, the number of SUEs required to initiate pump operation becomes dependent upon the time that has elapsed since the beginning of the discharge period. In the example system used to generate Fig. 7, for instance, it is clear that the only way to force the

pumps to re-energize during the first few minutes of the discharge period is for three usage events to occur in relatively short succession. If that does not happen, however, the leak will continue to reduce the pressure in the reservoir. Eventually, leak-induced loss will be large enough that only 2 SUEs are needed to initiate pump operation. For example, at the time t_0 shown in Fig. 7, it is clear that the pressure loss resulting from 2 SUEs will be sufficient to cause the pumps to energize.

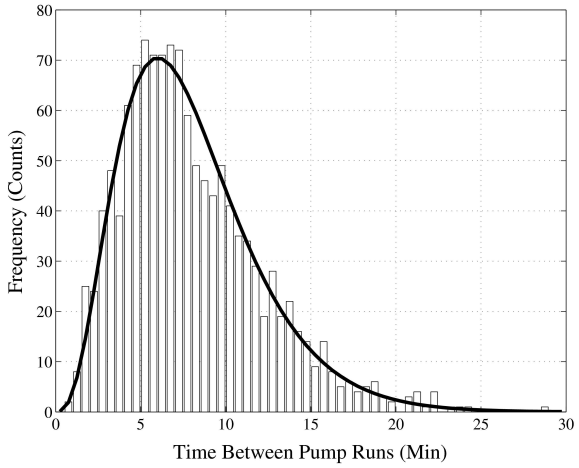

Figure 6: Expected (solid line) and simulated (bars) frequency distributions for the discharge time, T_p, when no leak is present in the idealized system. The simulation time was one week.

With certain simplifying assumptions, a more rigorous foundation can be provided for the leak behavior described above. Specifically, for a lumped element system, the time dependence of the leak-induced pressure loss can be described mathematically using the solution to Eq. 1. If the controller is programmed so that it keeps the pressure within a relatively narrow range, then the exponential solution to Eq. 1 can be represented using a first order Taylor series expansion, i.e. $P_{leak}(t) = \alpha_{leak}\, t$. For a system that obeys these assumptions, there are exactly N_{max} times at which the required amount of usage-induced pressure loss decreases. The procedure used to identify these times is outlined graphically in Fig. 8. As an example, consider what happens if the discharge period lasts until time τ_1. At that exact instant, the leak has reduced the pressure to the point that the

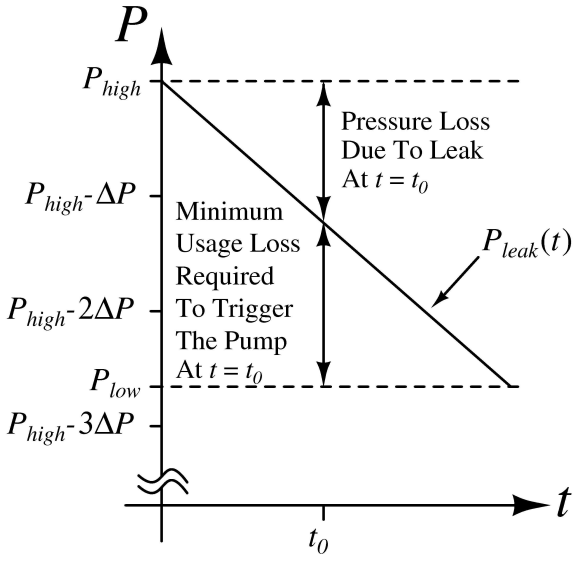

Figure 7: Leak-induced pressure loss versus time in an example system with N_{max}=3. Note that the distance between $P_{leak}(t)$ and P_{low} is the amount of usage-induced pressure loss that would be needed in order to cause the pump to energize at time t. Note that t has units of mintues.

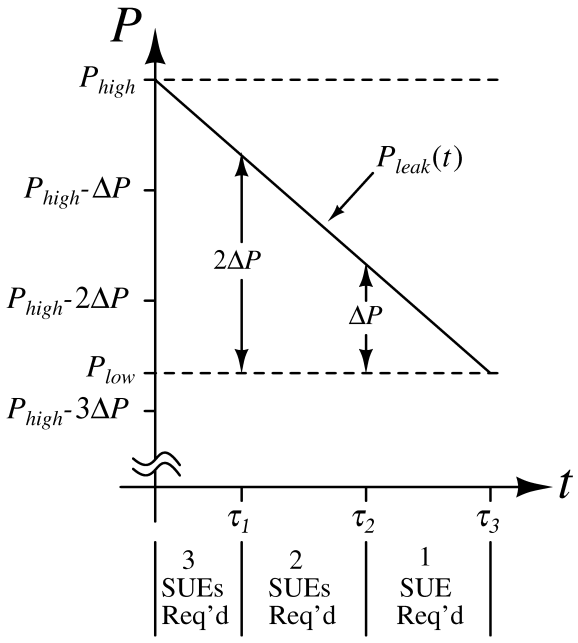

Figure 8: Leak-induced pressure loss versus time in an example system with N_{max}=3 and a linear pressure loss. Note that at time τ_1, the distance between $P_{leak}(t)$ and P_{low} is only $2\Delta P$, meaning that only 2 SUEs are required to trigger the pumps at that time. Similar behavior is observed at times τ_2 and τ_3. Note that t has units of minutes.

pumps will operate if the usage-induced loss is exactly $(N_{max}\text{-}1)\Delta P$. Prior to that time, however, only the occurrence of N_{max} SUEs could have forced the system pressure to fall below P_{low}. A similar procedure can be used to determine τ_2, the time at which the required usage loss drops from $(N_{max}\text{-}1)\Delta P$ to $(N_{max}\text{-}2)\Delta P$. In general, the values of the times τ_k are given by the formula

$$\tau_k = \frac{P_{high} - P_{low} - (N_{\max} - k)\Delta P}{\alpha_{leak}}, \quad \text{for } k = 1,2,\ldots,N_{\max}. \tag{12}$$

As a result of the effects described above, the distribution for the length of the discharge interval changes in the presence of a leak. Specifically, there is an additional probability that the pumps will run at the times τ_k. For instance, the pumps are guaranteed to run at τ_1 if exactly N_{max}-1 SUEs occurred prior to that time. As shown in (Mosman, 2006), $f_{T_p}(t)$ becomes

$$\begin{aligned} f_{T_p}(t) = {} & \frac{\lambda^{N_{\max}} t^{N_{\max}-1} e^{-\lambda t}}{(N_{\max}-1)!}\left[u(t) - u(t-\tau_1)\right] \\ & + \sum_{i=2}^{N_{\max}} \frac{\lambda^{N_{\max}-i+1} t^{N_{\max}-i} e^{-\lambda t}}{(N_{\max}-i)!}\left[u(t-\tau_{i-1}) - u(t-\tau_i)\right] \\ & + \sum_{i=1}^{N_{\max}-1} \Bigg[\frac{\lambda^{N_{\max}-i}}{(N_{\max}-i-1)!} \int_0^{\tau_i} t^{N_{\max}-i-1} e^{-\lambda t} dt \\ & \quad - \frac{\lambda^{N_{\max}-i+1}}{(N_{\max}-i)!} \int_0^{\tau_i} t^{N_{\max}-i} e^{-\lambda t} dt \Bigg] \delta(t-\tau_i) \\ & + \left[1 - \lambda \int_0^{\tau_{N_{\max}}} e^{-\lambda t} dt\right] \delta\left(t - \tau_{N_{\max}}\right) \end{aligned} \tag{13}$$

Figure 9 displays a simulated frequency distribution that was obtained by inserting a small leak into the ideal system characterized by the parameters presented in Table 1. The actual leak rate in this case is 10inHg/hr. Note that the additional probability of observing a pump run at the times τ_k results in the formation of large pulses at the those times. For comparison purposes, Fig. 9 also shows the frequency distribution that is predicted by Eq. 13.

CASE 2: TIME-VARYING λ, RANDOM ΔP

In reality, many cycling systems do not obey all of the assumptions used in Case 1. Most importantly, the pressure loss ΔP_k due to a single SUE will often be a random quantity. As a result, the number of SUEs required to initiate pump operation during normal conditions is no longer a fixed quantity. In this case, we state that the pump will energize immediately following the arrival of the η-th SUE, where η is a discrete-valued random variable whose value during any given discharge period is clearly dependent upon the amount of pressure removed by each of the SUEs that occurred during that discharge period.

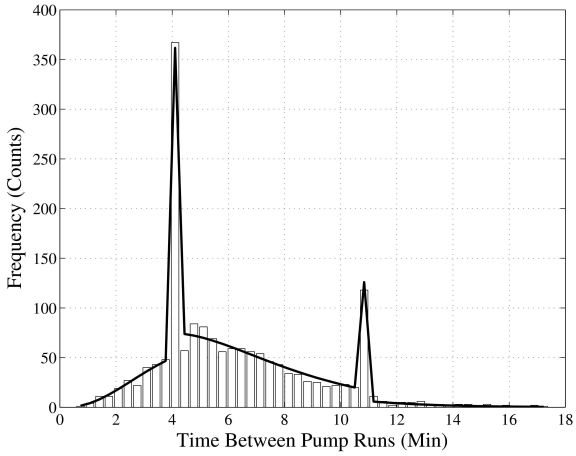

Figure 9: Expected (solid line) and simulated (bars) frequency distribution for the discharge time, T_p, in the idealized system with a 10inHg/hr leak rate. The simulation time was one week.

Under these conditions, the length of any individual discharge period is

$$T_p = T_1 + T_2 + \cdots + T_\eta. \tag{14}$$

Since T_p is now the sum of a random number of random variables, we can only derive its PDF by first deriving the distribution for ΔP_k. Using a short series of experiments and some fundamental physical reasoning, we determined that there are roughly two different ΔP_k values in the *Seneca*'s waste disposal system. Moreover, we discovered that there is a considerable amount of random variation about each of those values (Mosman, 2006). For simulation purposes, we assumed the following distribution for ΔP_k :

$$f_{\Delta P}(\Delta p) = \begin{cases} 5, & 0.6 \le \Delta p \le 0.7 \\ 5, & 1.3 \le \Delta p \le 1.4 \end{cases}. \tag{15}$$

Another issue in many real cycling systems is that the usage rate, λ, does not remain constant. For instance, it is reasonable to expect that the vacuum-assisted waste disposal system aboard an operational vessel will experience usage fluctuations throughout the day, as there are simply certain times when the crew is more likely to use the restrooms (i.e. at meal times or at watch changes). These fluctuations, which can be due both to deterministic and random effects, clearly impact the distribution for T_p. It is difficult, however, to establish a completely accurate model for the time-dependence of λ. In order to include this effect in our simulations, we studied our data from the *Seneca* to see if there were any obvious trends. During that process, we discovered that the average usage rate is different during each of the vessel's three watch shifts. On that basis, our simulation uses the following model for $\lambda(t)$

$$\lambda(t) = \begin{cases} \lambda_1, & 0h \le t < 8h \\ \lambda_2, & 8h \le t < 16h \\ \lambda_3, & 16h \le t < 24h \end{cases}, \qquad (16)$$

where t is in units of hours and t=0 is defined to be at midnight each day (Mosman, 2006). In reality, Eq. 16 does not completely reflect all of the random variation in the usage rate, as it would be difficult, if not impossible, to do so. As we will show, our current model is sufficient for developing powerful diagnostic indicators.

A third issue encountered in most real cycling systems is that the usage process will not reset each time the pump is de-energized. Specifically, the first inter-arrival time in Eq. 14 (i.e. T_1) will depend upon the time at which the last SUE occurred, which was either during the charging interval or during the previous discharge period. Although this fact has a rather minimal effect on the distribution for T_p, it is included for the sake of completeness.

In order to validate the more realistic behavior presented in this section, we developed a new simulation and compared the simulated results to measurements obtained by non-intrusively monitoring the *Seneca*'s waste disposal system (Mosman, 2006). The parameters values used in the simulation, which are presented in Table 2, were chosen following an analysis of the *Seneca*'s waste disposal system. The histogram presented in the top plot in Fig. 10 shows the simulated frequency distribution for T_p over a five-day period; the bottom histogram shows the measured frequency distribution over an equivalent time interval. Note the qualitative agreement between the two histograms.

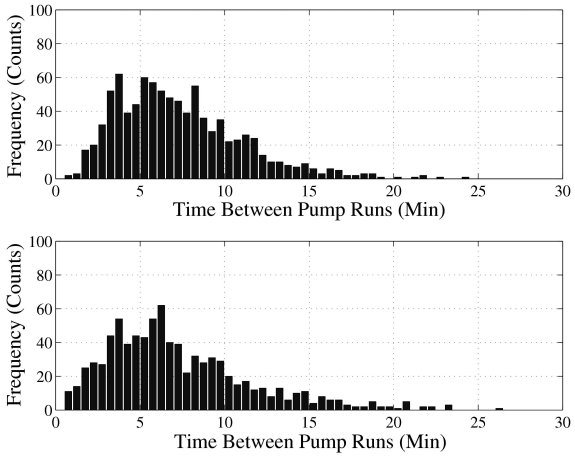

Figure 10: Simulated (top trace) and measured (bottom trace) frequency distributions for the discharge time, T_p, under normal (i.e. no leak) operating conditions.

Table 2: Parameters used in the modified system simulation.

Parameter	Value
P_{high}	17.5 inHg
P_{low}	13.5 inHg
λ_1	24 hr^{-1}
λ_2	36 hr^{-1}
λ_3	38 hr^{-1}
ΔP	See Eq. 15

When a leak is introduced into the realistic system described in this section, its effect on the distribution $f_{T_p}(t)$ is quite different than it was in the ideal case. Specifically, the large pulses shown in Fig. 9 will not appear in this situation. There are several reasons for this change. Most importantly, the random variation in ΔP_k will effectively "smear" these pulses over several different bins. To see this, once again consider the example system used to generate Fig. 8.

Recall that in that idealized system, each SUE removes the same amount pressure, meaning that the pump is guaranteed to enter operation at time τ_1 as long as 2 SUEs occurred prior to that time. Consider, however, what would happen if each usage event in that system did not remove the same amount of pressure from the reservoir. In that case, it is possible that exactly 2 SUEs could occur prior to time τ_1 and result in less pressure loss than what is required to trigger the pump at τ_1. As a result, the system will continue to discharge for an additional period of time after τ_1. Similarly, it is also possible that exactly 2 SUEs could occur prior to time τ_1 and result in more pressure loss than what is required to trigger the pump at τ_1. As a result, the pump will enter operation slightly earlier. Clearly, this behavior will effectively "spread out" the large pulses observed in the ideal case.

In our full simulation, we also included a time-dependent leak rate. To simulate this effect, we modeled the system using lumped element approximations and used the time-dependent loss model presented in Eq. 1. Without any system usage, Eq.1 predicts that the pressure loss will be a purely exponential function of time. In the presence of system usage, however, the leak rate will lessen slightly after each individual SUE, thus implying that the leak rate will change at random times. This effect will also cause the pulses observed in the ideal case to "spread" over several different histogram bins.

In order to verify the behavior of the model in the presence of a leak, we obtained several sets of both simulated and experimental data. For instance, Fig. 11 shows both simulated and measured frequency distributions for a leak with an initial rate equal to 12inHg/hr [1]. For the purpose of this comparison, we manually inserted a leak into the system using a small, adjustable flow meter.

[1] In this case, the term "initial leak rate" refers to the value of the leak rate at t=0, i.e. at the beginning of the discharge period. We make this distinction since the rate is considered to be a function of time.

As shown in Fig. 11, our simulated results are in qualitative agreement with the data obtained aboard the *Seneca*. Moreover, Fig. 11 demonstrates that the behavior of the real system in the presence of a leak is clearly not the same as that predicted by the idealized model considered in Case 1. Regardless, it is clear that the histograms in Fig. 11 are distinctly different than their "no leak" counterparts displayed in Fig. 10. In the next section of this paper, we present methods that can be used to detect these differences.

Figure 12 presents another set of validation data. In that case, the experimental results were obtained during a period when the *Seneca*'s waste disposal system was known to have a faulty check valve. Clearly, a leak this large is detectable.

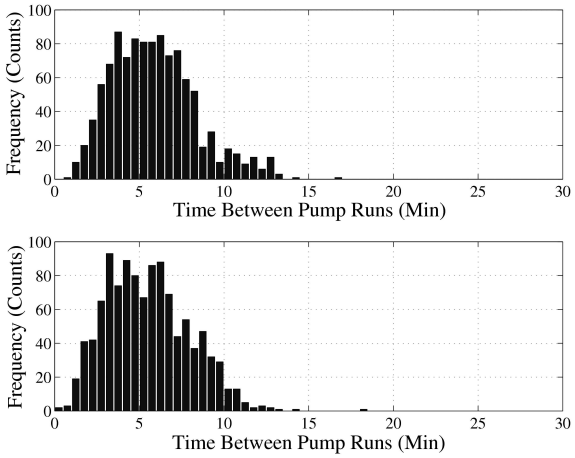

Figure 11: Simulated (top trace) and measured (bottom trace) frequency distributions for the discharge time, T_p, in the presence of a small leak. Both plots contain data collected over five days.

DIAGNOSTIC INDICATORS

As suggested by the model developed in the previous section, it is possible to detect leaks in cycling systems by searching for certain changes in the operating schedule of the system's pumping device. Since the NILM determines the operating schedule for each load on an electrical service, its diagnostic software can be easily designed to perform the necessary analysis.

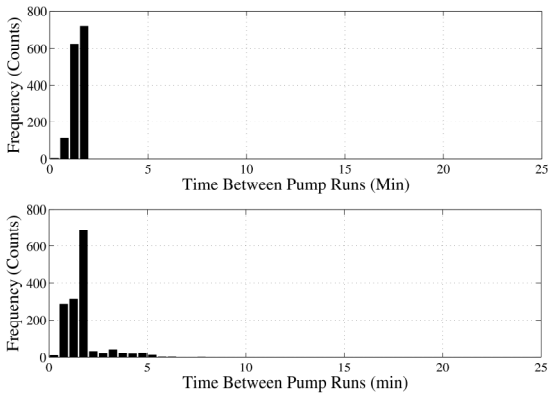

Figure 12: Simulated (top trace) and measured (bottom trace) frequency distributions for the discharge time, T_p, in the presence of a large leak. Both plots contain three days worth of data.

The cycling system diagnostic software that is currently installed on the NILM is implemented as shown in the flow chart in Fig. 13. The basic procedure is rather straightforward. At a pre-specified time each day, the NILM diagnostics module accesses the database that contains operating schedule information for each load on the monitored electrical service. The NILM then pulls all of the on/off times recorded for the relevant pump over the past three days. Subsequently, this data is analyzed using three different techniques, each of which is discussed in detail below. Using the results of the three analysis methods, the NILM decides whether or not a leak is present in the system. As discussed below, the NILM makes this determination using two different decision routines. Once the NILM has determined the current state of the system, it generates a status report that is both archived and sent via e-mail to the ship's Engineering Officer. In the remainder of this section, we present both the analysis routines and the decision-making methods that the NILM uses in order to detect fault conditions in cycling systems.

Analysis Methods

As indicated by the results presented in the previous section, different-sized leaks will affect the operating schedule of the system's pump in markedly different ways. Since shipboard cycling systems are subject to both small and large leaks, it is desirable to be able to detect both. In order to do so, however, our software must be equipped with techniques that are suitable for sensing small leaks and schemes that are suitable for detecting large leaks. When using the three methods described in this section, we have been able to detect all of the leaks that are of concern to the Engineering Officer aboard the *Seneca*.

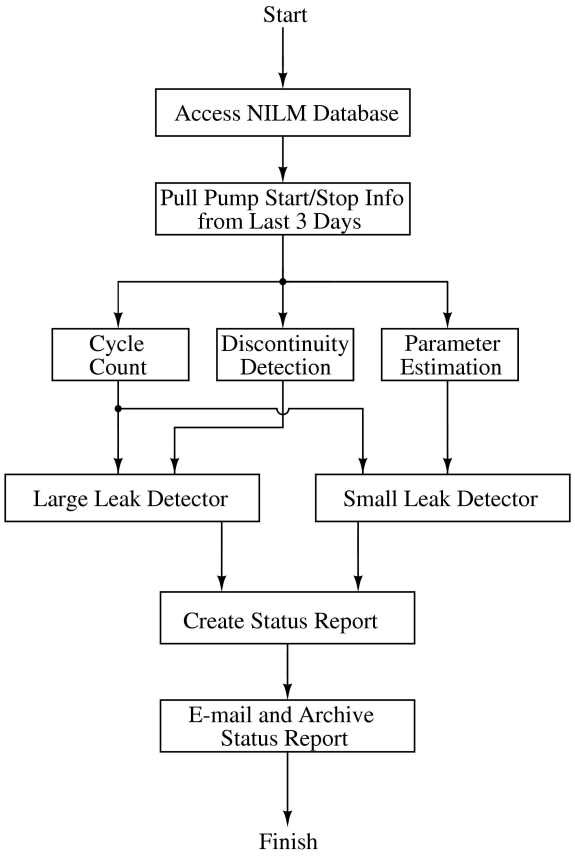

Figure 13: Fundamental flow chart for the NILM's cycling system diagnostic software. The final e-mail is sent to the ship's Engineering Officer.

CYCLE COUNT

Given that the operating schedule of the pumping device in a cycling system is strongly influenced by the operation of the system's air loads, one obvious method for detecting changes in the state of the system is to count how many times the pump has operated during a fixed time interval. It is important to note, however, that this procedure cannot definitively detect leaks, as increased system usage will also increase the

frequency of pump operation. Regardless, this method is very helpful when combined with the other two analysis procedures outlined below.

On any given day, we determine two different run count values. First, we compute what we call the one-day cycle count, which indicates the number of times that the pump has operated in the last 24 hours. Additionally, we calculate a three-day cycle count, which indicates the number of times that the pump has operated in the last three days. As we will show, the three-day cycle count is useful when detecting small leaks, as the inclusion of three days of data acts to smooth out daily fluctuations in usage.

DISCONTINUITY DETECTION

As shown previously, cycling system leaks distort the expected distribution for the discharge time, T_p. In the event that the system develops a leak as large as the one considered in Fig. 12, the effect will be the creation of a sharp edge in the measured histogram. The immediate detection of such edges is desirable, as leaks as large as the one used to generate Fig. 12 can result in excessive wear on the pumps.

If we view the measured histogram as a discrete-valued signal, $x[n]$, then we can detect the existence of any sharp edges using standard edge detection algorithms. In the cycling system diagnostics module, we locate sharp edges using the following procedure. First, we pass $x[n]$ through a five-point median filter and store the results in the vector $y[n]$. Subsequently, we compute $| y[n]-x[n] |$ and determine if the result exceeds a preset threshold at any value of n. If so, it is highly likely that a leak is present in the system.

PARAMTER ESTIMATION

As suggested by both the simulated and measured results presented in Fig. 11, small leaks also distort the distribution for the discharge time, T_p. Clearly, however, the distortion is not as visually distinct as it is when the system develops a very large leak. In order to detect these small but potentially crippling fault conditions, we must turn to other methods.

In order to aid in the detection of small leaks, the NILM diagnostics software attempts to fit the measured discharge time data to a pre-specified model. As shown in (Mosman, 2006), one model that has been found to fit real data is the gamma distribution, which is a generalization of the ideal PDF presented in Eq. 11 (Hahn, 1994). Mathematically, this two parameter distribution is given by the equation

$$f_{T_p}(t) = \frac{\lambda^k t^{k-1} e^{-\lambda t}}{\Gamma(k)}, \tag{17}$$

where

$$\Gamma(k) = \int_0^\infty t^{k-1} e^{-t} dt\,. \tag{18}$$

In order to obtain estimates for the parameters k and λ, the NILM currently uses the maximum-likelihood estimation routine that is built in to MATLAB (Hahn, 1967). Based on numerous simulations and field tests, we have determined that three days worth of pump on/off data represents a reasonable statistical sample (Mosman, 2006).

As we show in the Results section, both k and λ tend to increase when leaks are inserted into both the real and simulated systems. Furthermore, similar trends have not been observed when the usage rate increases. It is important to note that in this context, the parameter λ does not refer to the system's usage rate; rather, it is simply an indicator of the scale of the measured distribution (Hahn, 1994). As described in (Hahn, 1994), the simultaneous horizontal narrowing and vertical growth experienced by the measured distribution during leak conditions will result in an increase in the estimated values for both k and λ. For analysis purposes, the NILM stores its daily parameter estimates.

Decision Methods

Once the operating schedule of the pump has been analyzed using the three procedures described above, the NILM decides whether or

not a fault is currently present in the cycling system. In order to make this determination, the NILM uses two different decision-making routines. If either of these routines determines that a leak is present in the system, the NILM will indicate this fact to the Engineering Officer in its daily status report.

LARGE LEAK METHOD

The first decision-making routine contained in the NILM's cycling system diagnostic software determines if any large leaks are present in the system. During both our field studies and simulations, we have found that such leaks distort the operating schedule so strongly that they can be detected using data obtained over a single, 24-hour period (Mosman, 2006).

To check for large leaks, the NILM proceeds in two steps. First, it determines if there has been a significant change in the number of times that the pump has operated over the past 24 hours. To do so, it uses the output of the one-day cycle counting procedure described above. If the number of pump runs observed in the past 24 hours exceeds the average number observed over the past three days, then the NILM will check the output of the discontinuity detector to see if the histogram has developed any sharp edges. If so, the NILM will immediately alert the Engineering Officer that the system has developed a leak.

SMALL LEAK METHOD

The second decision-making routine contained in the NILM's cycling system diagnostic software determines if any small leaks are present. During both our field studies and simulations, we have found that such leaks require a relatively large statistical sample in order to be detected. Thus, in this case, we make our decision using three days of pump on/off data (Mosman, 2006).

To check for small leaks, the NILM again proceeds in two steps. First, it uses the three-day cycle count to determine if there has been a change in the number of times that the pump has operated over the past several days. To do so, the NILM applies a simple, FIR filter-based change-of-mean detector to the three-day cycle count. If the mean has changed by a certain preset threshold, then the NILM will proceed to its second step, which is to examine the parameter estimates obtained during the estimation procedure. If both the estimated k and λ values exceed pre-determined thresholds, then the NILM will indicate to itself that a small leak may be developing in the system. For the next several days, the NILM will continue to monitor the estimated k and λ values. If these values remain at or near their alarm levels for at least two days, then the NILM will alert the Engineering Officer that it is likely that a small leak is present in the system.

RESULTS

The diagnostic methods discussed above were tested using both simulated and measured data. The purpose for using synthetic and real data was to demonstrate both the validity of the fundamental cycling system model and the efficacy of the diagnostic indicator methods.

Simulated Data

LARGE LEAK METHOD

To test our large leak indicator, we applied it to a single day of the simulated data used in Fig. 12. Figure 14 shows the resulting output of the discontinuity detector described above. In this case, the data exceeds the preset threshold and a leak is successfully detected. For reference, the threshold is set to 150.

SMALL LEAK METHOD

To test the small leak detection method, we used our simulator to generate a 34-day data set that includes both a period of elevated usage and a period in which a leak is present. Both the three-day cycle count and the parameter estimates for this data are shown in Fig. 15. At the outset of both the leak conditions and the period of elevated usage, the NILM detected a

change in the number of pump runs. In the case of the leak, the NILM signaled a fault condition on Day 12, as both the estimated k and λ values exceeded their alarm thresholds for the required two days. In the case of elevated usage, however, the parameter estimates never exceeded their thresholds, and no warnings were provided. For reference, the alarm thresholds for k and λ are set at 5 and 1 min^{-1}, respectively.

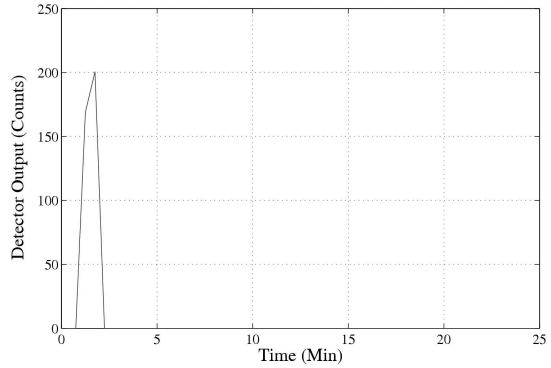

Figure 14: Output of the discontinuity detector when using a single day of the simulated data plotted in Fig. 12. Since the difference between the actual data and the median filter output exceeds the threshold (150), a leak is signaled.

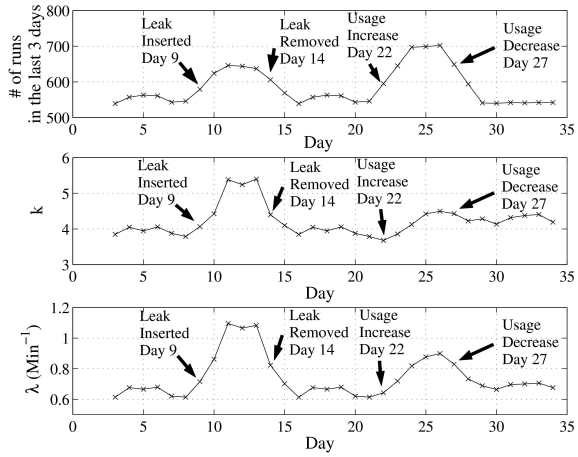

Figure 15: Simulated data used to test the small leak detection method.

Measured Data

LARGE LEAK METHOD

The large leak detection scheme has been used to sense actual fault conditions in the vacuum-assisted waste disposal system aboard the *Seneca*. Figure 16 shows the histogram created by the NILM on a day in which the check valve in the suction port of the vacuum pump failed. The large leak detection method easily discovered this fault, and the Engineering Officer was immediately notified. During our research, we have found that such leaks can often go undetected for days or even weeks, thus seriously jeopardizing the health of the pumps.

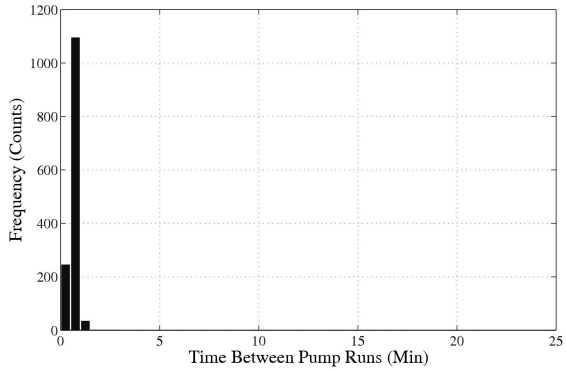

Figure 16: Measured frequency distribution on the first day of a check valve failure in the *Seneca*'s waste disposal system. Our software easily detects this potentially crippling leak.

SMALL LEAK METHOD

The small leak detection procedure has also been tested on the vacuum-assisted waste disposal system aboard the *Seneca*. To test this scheme, the crew of the *Seneca* inserted several small leaks into the system using an adjustable flow meter that we provided to them. Following our experiments aboard the ship, we constructed a 65-day data set that contains two periods in which the system is affected by a leak with an initial rate of approximately 12inHg/hr. Figure 17 shows the daily evolution of both the three-day cycle count and the parameter estimates obtained for this data. In this case, the NILM successfully identified a leak on both Day 30 and on Day 46. For reference, the alarm thresholds applied to real data are 4.2 (for k) and 0.7min^{-1} (for λ).

It is important to note that the measured data also displays a slight amount of usage variation. In particular, the change-of-mean detector noticed a change in the three-day cycle count on Day 8. Since the parameter estimates never

exceeded their alarm levels, however, the NILM ignored the change.

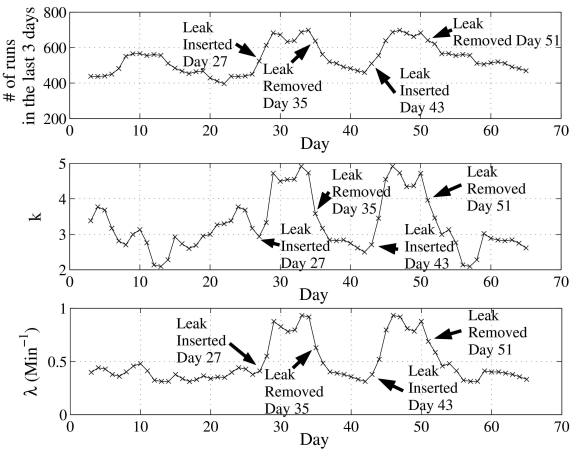

Figure 17: Measured data used to test the small leak detection method.

CONCLUSIONS

This paper has shown that the NILM is capable of detecting the presence of fault conditions in shipboard cycling systems. The diagnostic indicators presented here were developed using a simple physical model, and they were validated using both simulated and measured data. The cycling system model proposed in this paper indicates that our diagnostic tools can be applied not only to the example system, but also to any cycling system showing the same general behavior. At present, we are continuing to test and to develop our diagnostic software.

REFERENCES

Bertsekas, D.P. and Tsitsiklis, J.N. *Introduction to Probability.* Belmont, MA: Athena Scientific, 2002.

DeNucci, T. et al. "Diagnostic Indicators for Shipboard Systems Using Non-Intrusive Load Monitoring," in *Proc. of 1st IEEE Electric Ship Technologies Symposium.* Philadelphia, PA. July 2005.

DiUlio, M., Savage, C. and Schneider, E. "Taking the Integrated Condition Assessment System into the Year 2010," *13th Ship Control Symposium,* Orlando, FL, 2003.

Greene, W. et al. "Non-Intrusive Monitoring for Condition-Based Maintenance," in *Proc. of ASNE Reconfiguration and Survivability Symposi.* Atlantic Beach, FL. February. 2005.

Hahn, G.J. and Shapiro, S.S. *Statistical Models in Engineering.* New York: Wiley, 1994.

Mosman, J. P. "Evaluation of Non-Intrusive Load Monitoring for Shipboard Cycling System Diagnostics," NE/SM Thesis, MIT, Cambridge, MA, June 2006.

Ramsey, J. S. et al. "Shipboard Applications of Non-Intrusive Load Monitoring," in *Proc. of ASNE Reconfiguration and Survivability Symposium.* Atlantic Beach, FL. February. 2005.

Shaw, S.R., "System Identification Techniques and Modeling for Nonintrusive Load Diagnostics," Ph.D. Dissertation, MIT, Cambridge, MA, February, 2000.

Tijms, H.C. *A First Course in Stochastic Models.* Hoboken, NJ: Wiley, 2003. .

Robert Cox; **Lt. James P. Mosman, USN; and LCdr. Duncan McKay, USN** *are graduate students in the Laboratory for Electromagnetic and Electronic Systems at MIT.*

Dr. Steven B. Leeb *received S.B., S.M., E.E. and Ph.D. degrees from MIT. He has been a member of the MIT faculty in the Department of Electrical Engineering and Computer Science since 1993. He serves as a professor in the Laboratory for Electromagnetic and Electronic Systems.*

CDR Timothy J. McCoy, **USN** *holds a Ph.D., Naval Engineer and a master's in Electrical Engineering from MIT and a bachelor's degree in Mechanical Engineering from the University of Illinois. He has worked on the designs for the AOE-6, LPD-17 and DD(X) ship classes as well as the Integrated Power System (IPS) and Standard Monitoring & Control System (SMCS) development programs.*